Chemical Engineering Journal 474 (2023) 145867

Contents lists available at ScienceDirect

Chemical Engineering Journal

journal homepage: www.elsevier.com/locate/cej

Highly efficient non-doped deep-blue organic light-emitting diodes based on pyreneimidazole derivative with external quantum efficiency > 11% and negligible efficiency roll-off

Zhuang Cheng [a], Chunya Du [a], Shuyuan Ge [a], Yaxue Wang [a], Futong Liu [a], Yulei Chang [b], Ying Lv [b], Ping Lu [a,*]

[a] State Key Laboratory of Supramolecular Structure and Materials, Institute of Theoretical Chemistry, College of Chemistry, Jilin University, Changchun 130012, China
[b] State Key Laboratory of Luminescence and Applications, Changchun Institute of Optics, Fine Mechanics and Physics, Chinese Academy of Sciences, Changchun 130033, China

ARTICLE INFO

Keywords:
Pyreneimidazole derivative
Deep-blue emitters
Hot exciton
Low efficiency roll-off
PhOLEDs

ABSTRACT

The development of highly efficient deep-blue fluorescent materials applicable in non-doped organic light-emitting diodes (OLEDs) is still an appealing yet challenging task. Herein, we present a rational design of deep-blue material, PyPO, by linking pyreneimidazole (PyI) moiety with diphenyl ether unit through a benzene bridge. A weak charge transfer state between PyI and diphenyl ether in PyPO is observed from the photophysical investigation, and it is provided with the hybridized local and charge transfer (HLCT) feature as indicated by theoretical calculations. The neat thin film of PyPO shows high photoluminescence quantum yield (PLQY) of 70.7% and excellent horizontal dipole ratio of 84.0%, respectively. In particular, the non-doped OLED using PyPO as the active layer exhibits an electroluminescent (EL) emission peak at 448 nm with an impressive maximum external quantum efficiency (EQE) of 11.1% and negligible roll-off at 1000 cd m^{-2}, which is one of the best results among PyI-based deep-blue luminogens. In addition, the red phosphorescent OLED applying PyPO as host achieves a maximum EQE of 31.3% and still remains 28.6% at 1000 cd m^{-2}, demonstrating PyPO is also a suitable phosphorescent host material. The excellent device performance is ascribed to the high-lying reversed intersystem crossing (hRISC) via hot exciton mechanism. These findings may provide new insights for the development of highly efficient deep-blue emitters.

1. Introduction

Organic light-emitting diodes (OLEDs), with the intrinsic merits of flexibility, light-weight, wide angle, ultra-thin, etc., have been extensively investigated and commercially applied in a wide range of display products such as smartphones and TV screens as well as in panels for lighting in recent years [1–4]. High-efficiency blue, green and red materials are the fundamental components for constructing OLEDs. However, in commercial OLED applications, inefficient blue fluorescence OLEDs usually work in tandem with efficient green and red phosphorescence OLEDs (PhOLEDs), which severely affects the color accuracy and increase the energy consumption of the whole screen [5–8]. The pursuit for deep-blue luminogens exhibiting a Commission Internationale de L'Eclairage (CIE) y coordinate below 0.15 and a total (x + y) value under 0.30 is crucial to further improve the quality of vivid display [9,10]. Besides serving as one of the primary components for OLEDs, deep-blue emitters also can serve as energy donors to yield other visible emissions and white lightings through energy transfer processes [11,12]. High-efficiency OLEDs are frequently fabricated using a doping process, which necessitates using an appropriate host material and fine-tuning the doping concentration [13–15]. This will inevitably complicate the manufacturing of devices and raise their commercial cost. A single layer of non-doped emitters exhibits considerable advantages in terms of dependability, simplicity, and inexpensive manufacturing costs [16]. Hence, it is highly important to develop deep-blue luminogen with the capability to achieve high performance in non-doped OLEDs.

According to the limitation of spin statistics, 25% of the excitons are created in the singlet state and 75% of the excitons are in the triplet state [17–19]. All triplet excitons may be obtained by green and red phosphorescent materials, which have been commercially marketed for

* Corresponding author.
E-mail address: lup@jlu.edu.cn (P. Lu).

https://doi.org/10.1016/j.cej.2023.145867
Received 30 June 2023; Received in revised form 15 August 2023; Accepted 3 September 2023
Available online 4 September 2023

decades. These materials are often Ir- or Pt-based complexes [20–22]. To reduce the long-lived triplet excitons' tendency to quench and prevent reverse energy transfer from the dopant to the host in devices, they should be distributed into appropriate host materials with high triplet energy [23,24]. In light of the enhanced nonradiative process via d orbitals of metals when boosting the metal–ligand charge transfer (MLCT) state into the deep-blue zone, some limited success has also been shown in effective deep-blue phosphorescent dyes with high triplet energy levels. For conventional fluorescent materials, triplet excitons are not involved in the electroluminescence (EL) process [25–28]. To obtain 100% exciton utilization efficiency (EUE) in fluorescent materials, the triplet excitons must be used, hence an appropriate channel must be made in order to allow the singlet to pass back into the system in the reverse direction [29–32]. One of the most effective methods for enhancing EUE and EL performance has been proven to be creating emitters with a donor–acceptor (D-A) molecular configuration [33–35]. The thermally activated delayed fluorescence (TADF) and hot exciton materials with D-A structure using the triplet excitons in the form of radiative transitions via different ways have emerged after years of endeavors [36,37]. Based on the identical charge transfer (CT) character of the lowest triplet excited state (S_1) and the lowest singlet excited state (T_1), the RISC process happens in TADF materials from T_1 to S_1, which often leads to a relatively small spin–orbit coupling (SOC) value and low RISC rate constant [38–41]. The hot exciton material entails a relatively quick RISC from the high-lying triplet state (T_n, $n > 1$) to the excited singlet state (S_m, $m \geq 1$) in contrast to the conventional TADF process [30,42–44]. Besides, this process can weaken the gathering of triplet excitons and avoid the exciton annihilation of OLEDs to a great extent, laying the foundation for fabricating OLEDs by non-doping technology [44–47]. Thus, the hot exciton material with mild CT feature shows high potential in achieving deep-blue OLEDs with high efficiencies and low efficiency roll-offs in non-doped OLEDs [48–50].

Among various deep-blue materials, imidazole unit has attracted wide attention owing to the short conjugation and bipolar charge transport nature [9,25,26,28,51,52]. In prior work, fusing imidazole with planar π system such as pyrene could afford the π-extended motif of pyreneimidazole (PyI), which generally endows the related derivatives with reduced nonradiative vibrational and rotational processes, higher emission efficiency, and better thermal stability[9,51,52]. However, using the PyI moiety in blue emitters has shown moderate progress with emission in sky blue to greenish blue zones and maximum external quantum efficiencies (EQEs) less than 9% in non-doped device. The deep-blue emitters based on PyI group with CIE y coordinate value lower than 0.15 remain very limited. Aiming at blue-shifting the emission wavelength, the molecular conjugation degree and the intensity of CT should be rationally controlled. A judicious molecular design strategy can be expected by properly regulating the conjugation of the molecules and inducing suitable intermolecular interactions to give rise to high photoluminescence quantum yield (PLQY) as well as high horizontal dipole orientation simultaneously [53].

Here, a fluorescent material PyPO is constructed by selecting diphenyl ether as the weak electron donor and incorporating it with PyI at the N1 position of imidazole ring. In this approach, a weak CT excited state between PyI and diphenyl ether can be induced, which can ensure the deep-blue emission, enhance the formation of LE state and promote fluorescence efficiency. A benzene ring is also introduced to adjust the twisted angel between PyI and diphenyl ether to suppress the aggregation effect in solid films. The neat thin film of PyPO shows high horizontal dipole ratio of 84.0% and high photoluminescence quantum yield (PLQY) of 70.7%, respectively. The optimized non-doped OLED adopting PyPO as the emissive layer achieves an EL peak at 448 nm, impressive EQE of 11.1%, and almost negligible roll-off at 1000 cd m^{-2}. The doped device shows the CIE coordinates of (0.15, 0.07), which matches well with the NTSC standard CIE (x, y) coordinates of (0.14, 0.08) for deep-blue emitter. Moreover, red PhOLEDs applying PyPO as the host are also fabricated and acquire a maximum EQE of 31.1%, which realize the efficient utilization of the triplet exciton. The results offer a new design strategy for high-efficiency deep-blue luminogens as well as a suitable host for PhOLEDs to provide excellent EL performance.

2. Results and discussion

2.1. Synthesis and characterization

The synthetic route of the PyPO was shown in Scheme 1. As indicated by our previous work [9], the intermediate compound of PyPBr was prepared by a one-pot reaction, followed by boronization with bis (pinacolato)diboron to attain PyPB. And then, Suzuki coupling reaction between PyPB and 4-bromobiphenyl ether afforded the target molecule PyPO. The molecular structure was completely characterized using elemental analysis, ^1H and ^{13}C nuclear magnetic resonance (NMR) spectroscopy, mass spectrometry (MS) and the results were in well agreement with the expected structure (Fig. S1).

2.2. Thermal and electrochemical properties

The thermodynamic property of PyPO was investigated using thermogravimetric analysis (TGA) and differential scanning calorimetry (DSC) methods. As shown in Fig. 1(a), the thermal decomposition temperature (T_d) was 410 °C. PyPO exhibited a weak absorption peak at 103 °C, which could be assigned to the glass transition temperature (T_g). The good thermal stability guaranteed the vaporization in the device fabrication process. The electrochemical characteristics of PyPO were ascertained by cyclic voltammetry (CV) measurement, and results were illustrated in Fig. 1(b). The electrochemical curve in the forward and negative scans indicated that both electrochemical oxidation and electrochemical reduction processes occurred on the PyI group. The highest occupied molecular orbital (HOMO) energy level, which equated to the oxidation onset potential of 0.72 V, was −5.50 eV. The reduction onset potential of PyPO (−2.25 eV) was used to calculate the lowest unoccupied molecular orbital's (LUMO) energy level, which was calculated to be −2.48 eV. The electrochemical bandgap (E_g) was thus calculated to be 3.02 eV.

2.3. Theoretical calculation

To further understand the frontier molecular orbitals and molecular configuration of PyPO, the Gaussian 09 package was employed to simulate on the M06-2X/6-31G (d, p) basis set using density flooding theory (DFT) and time-dependent DFT (TD-DFT). As shown in Fig. S2, it was demonstrated that the PyPO's HOMO primarily concentrated on the PyI unit with an extension to the nearby benzene ring, and there was almost no distribution on biphenyl ether unit. The LUMO diffused to biphenyl ether group in a sizable amount and eventually delocalized on almost the entire molecule. The optimized molecular geometry of ground state was depicted in Fig. S3. PyI unit and the adjacent benzene showed a torsion angle of 29.9°, while the benzene bridge and biphenyl ether showed a torsion angle of 35.6°, respectively. Such small torsion angles contributed to the increasement of overlap between the HOMO and LUMO, which is also beneficial to improving optical out-coupling efficiency.

The natural transition orbitals (NTOs) were further determined in order to investigate the excited state properties. As seen in Fig. 2, the S_1 state's hole and particle distribution was mostly on the PyI unit and the adjacent benzene, and it exhibited the typical LE state's characteristics. The hole and particle of T_1 and T_2 states exhibited distribution similar to S_1. In comparison, the hole and particle of T_3 extended conjugation to biphenyl ether showing a partially overlapped distribution which was considered as the typical HLCT state. Additionally, Fig. S5 exhibited the energy levels of the first 10 singlet and triplet states calculated on the basis of M06-2X/6-31G (d, p). According to the energy diagram, the energy gap between S_1 and T_1 was as large as 1.15 eV. Therefore, from

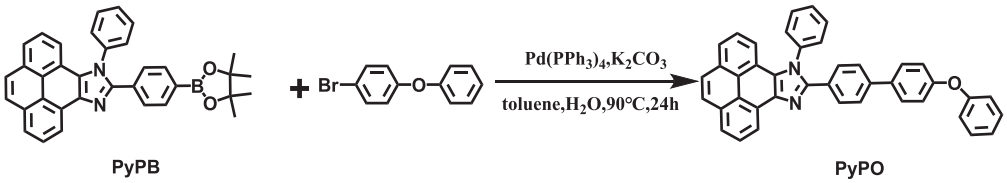

Scheme 1. The synthetic routes of PyPO.

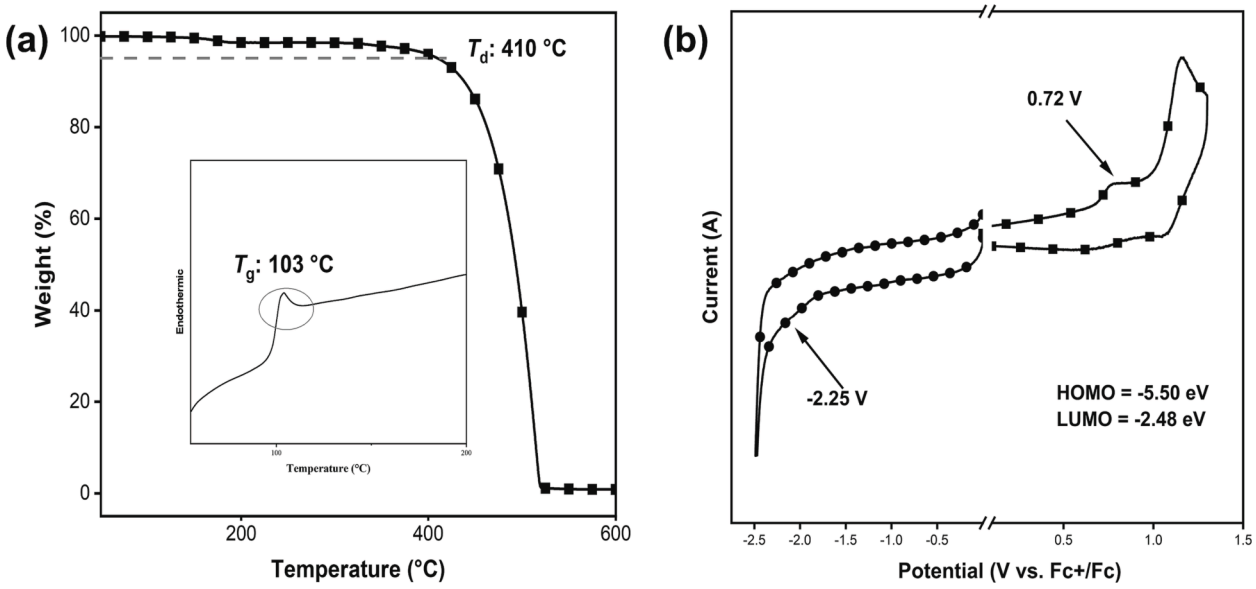

Fig. 1. (a) TGA and DSC (insert) curves for PyPO. (b) Cyclic voltammograms for PyPO.

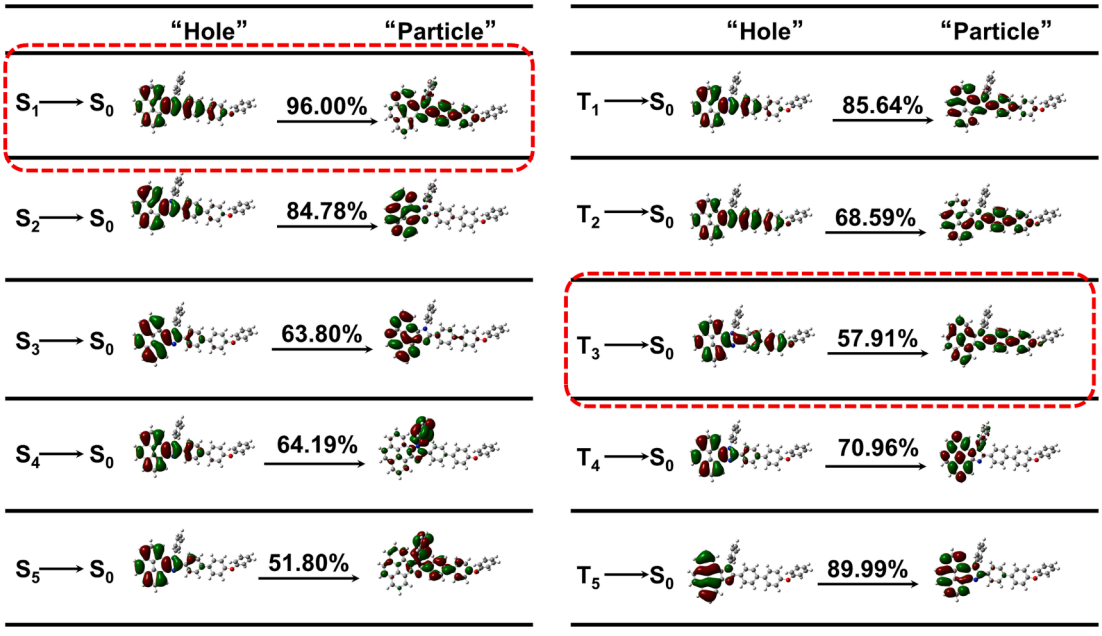

Fig. 2. Natural transition orbitals (NTOs) of PyPO.

T_1 to S_1, realizing RISC was not a facile process. In contrast, the energy levels of S_1 (3.34 eV) and T_3(3.41 eV) were calculated and their energy gap was only 0.07 eV, which might open a pathway for high-lying RISC (hRISC) from T_3 to S_1. Furthermore, according to the energy gap law, the energy gaps between $T_3 \rightarrow T_2/T_1$ and $T_1 \rightarrow S_1$ were large enough, which could minimize the internal conversion of $T_3 \rightarrow T_2/T_1$ and make it difficult for the RISC from $T_1 \rightarrow S_1$ [54].

2.4. Photophysical properties

The normalized UV–vis absorption spectra and fluorescence spectra of PyPO were determined in dilute solutions and neat films on quartz

substrates. As can be seen in Fig. 3(a), the absorption spectra exhibited a vibronic fine structure among 330 ~ 360 nm in THF, which could be ascribed to the multiple π-π* transition of the PyI unit. The short wavelength absorption band at 280 nm with high absorption intensity was also observed, corresponding to the benzene groups' transitions. The optical bandgap was 3.11 eV estimated from the onset of the absorption spectra.

The fluorescent spectra of PyPO showed the emission peak at 420 ~ 430 nm in different solvents. PyPO showed a high PLQY of 90.1% in THF. In particular, the vibrational fine structure was clearly visible in the low-polarity solvents and blurred as the polarity of the solution increased, and vibrational fine structure largely disappeared in the acetonitrile. With increasing solvent polarity, the emission spectra showed a little red-shift of 10 nm, along with a broadening of the full width at half maximum (FWHM) of the spectra, suggesting that PyPO had weak CT properties in the excited state. Further study of the solvatochromic effect was carried out by plotting a linear fit analysis based on the Lippert-Mataga solvatochromic model for Stokes displacement and solvent orientation polarizability and depicted in Fig. S6. The properties of excited states varied in low- and high-polarity solvents and the fitted curves for PyPO exhibited a two-step linear fit, corresponding to the LE state in low-polarity solvents with a small dipole moment (5.44 D) and the CT state in high polarity solvents with a steep slope (19.72 D). As a result of the coupling and intercrossing between the LE and CT states, the HLCT state was created.

PyPO's low temperature fluorescence and delayed phosphorescent spectra at 77 K were determined and depicted in Fig. 3(c). The matching emission peaks were found at 405 nm and 568 nm, respectively, which corresponding to the S_1 energy level of 3.06 eV and the T_1 energy level of 2.18 eV. Obviously, RISC between S_1 and T_1 was not allowed on account of such a large energy gap ($\Delta E_{ST} = 0.88$ eV). Fig. 3(d) depicted transient PL decay curves in some solvents at 430 nm at room temperature to investigate the lifetime of excitons. The fluorescence decay exhibited a nano-second fluorescence decay in various solvents, which could be attributed to the fast radiative transition. Based on the PLQY and lifetime data, the radiative rate (k_r) of PyPO was calculated to be 4.03×10^8 s^{-1} and nonradiative transition rate (k_{nr}) was 4.1×10^7 s^{-1}, respectively. The photophysical properties in the solid state was also investigated. The non-doped thin film of PyPO exhibited single emission with the peak at 452 nm and the PLQY reached 70.7% (Fig. S7). The PLQY of the doped film was determined with the 10 wt% concentration of 4,4′-bis (carbazol-9-yl) biphenyl (CBP). The doped film exhibited a PLQY of

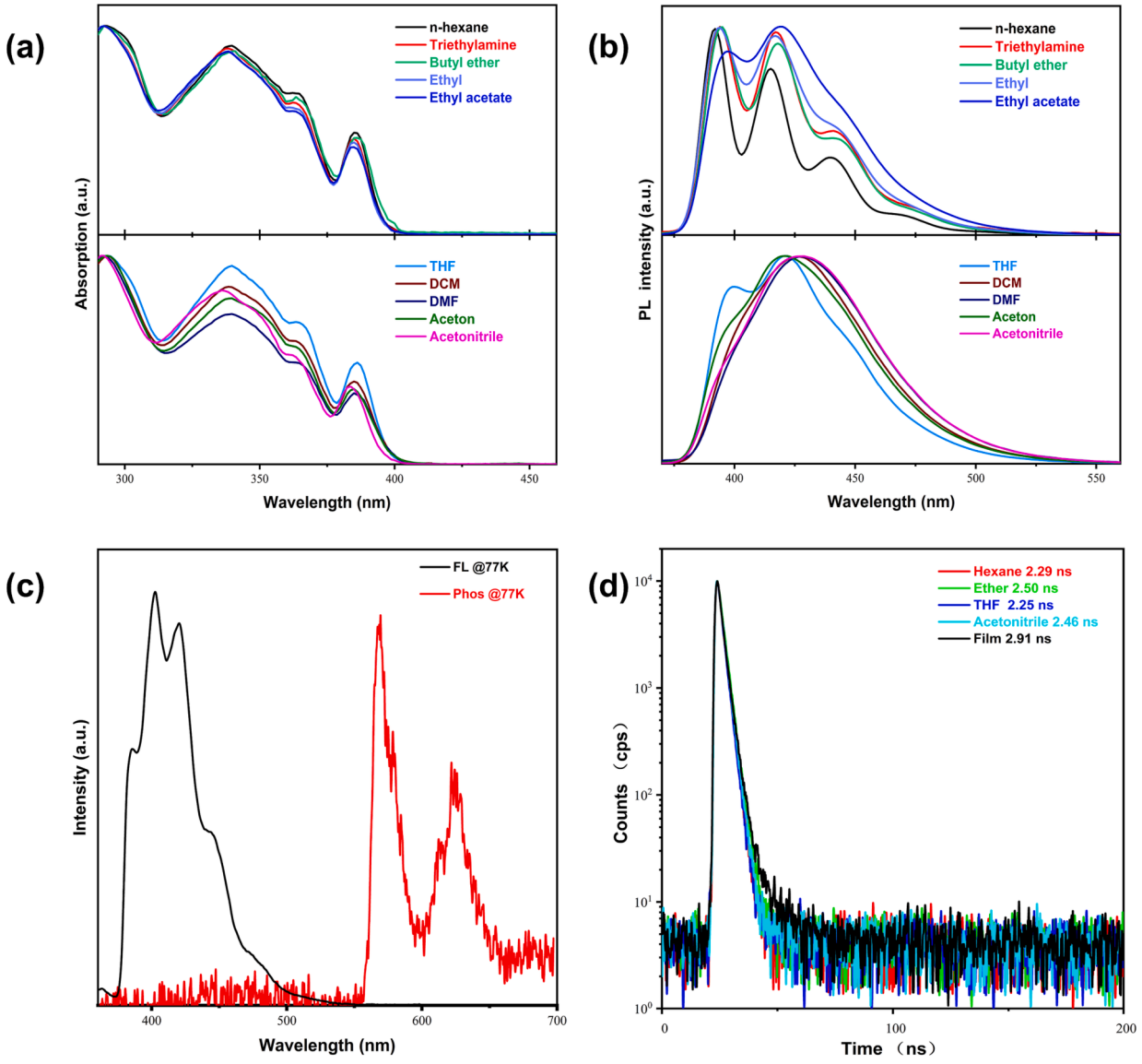

Fig. 3. (a) Absorption and (b) emission spectrum of PyPO in different solvents. (c) Fluorescence and phosphorescence spectrum at 77 K of PyPO. (d) Transient decay PL spectra of PyPO in different solvents with concentration of 1.0×10^{-5} M and neat film.

61.5%. In addition, the horizontal dipole ratio of the PyPO was investigated by measuring angular dependent p-polarized PL intensity, which was positively correlated with η_{out}. The neat thin film of PyPO furnished an excellent horizontal dipole ratio of 84.0%, and the optical outcoupling efficiency might be greatly increased with such a large horizontal dipole ratio (Fig. S8). In the excited state dynamics study, the emitter exhibited fast radiative decay rates exceeding 10^8 s^{-1}, which was nearly 10 times higher than the non-radiative decay rates. The rigid structure of PyPO can effectively suppress the energy dissipation of radiative decay processes and obtain high efficiencies. The key parameters were summarized in Table 1.

2.5. Electroluminescence properties

To investigate the potential of PyPO, we first employed non-doped devices and doped devices in Fig. 4 with the device structure of ITO/HATCN (6 nm)/TAPC (30 nm)/TCTA (10 nm)/EMLs (20 nm)/TmPyPB (40 nm)/LiF (1 nm)/Al (120 nm), in which indium tin oxide (ITO) and aluminum was adopted as cathodes; 1,4,5,8,9,11-hexaazatriphenylenehexacarbonitrile (HATCN) was the hole injecting layer; di-(4- (N, N-ditolyl-amino)-phenyl) cyclohexane (TAPC) worked as the hole transporting layer; tris(4-carbazoyl-9-ylphenyl)amine (TCTA) served as the excitons blocking layer; 3,3′-[5′-[3-(3-pyridinyl)phenyl][1,1′:3′,1′′-terphenyl]-3,3′′-diyl]bispyridine (TmPyPB) and lithium fluoride (LiF) functioned as the electron transporting layer and electron injection layer, respectively. EMLs represented PyPO in non-doped device and CBP:10 wt% PyPO in the doped device, respectively.

Fig. 5 and Table 2 both included a list of the key performances. The deep-blue emission corresponding to the CIE coordinate of (0.15, 0.13) was presented and the optimized non-doped device turned on at low voltage of 2.8 V, demonstrating the highly efficient carrier injection and transport within the device. The electrical charge injection procedure was confirmed by the EL spectrum's stability under a range of driving voltages without vibronic fine features, exhibiting outstanding color stability (Fig. S9). Particularly, the maximum EQE could be up to 11.1% and the device demonstrated a minor efficiency roll-off of 0.9% and 27.9% at 1000 cd m^{-2} and 10000 cd m^{-2}, respectively. And then, CBP was chose as the host to fabricate the doped device. With the 10 wt% doping concentration, the device exhibited an EL peak at 432 nm with a maximum EQE of 7%. With blue-shifted emission, the device revealed a CIE coordinate of (0.14, 0.07), surpassing NTSC deep-blue standard.

The EUE of the non-doped device exceeded the limit of 25%. The high EUE demonstrated the presence of triplet state excitons trapping. The mechanism of luminescence was examined to determine if the triplet–triplet annihilation (TTA) process predominated in the high EQE. The luminance increased linearly with current density, demonstrating that neither long-lived excitons nor current-induced fluorescence quenching significantly contributed to the EL process. Furthermore, transient EL spectra based on PyPO was also determined and shown in Fig. S10. After the removal of electrical excitation, the EL intensity of non-doped device decayed rapidly with a small delay component. The delayed component, which deviated from the TTA process's pattern, showed no apparent voltage dependence, which suggesting that the trapped charges' collisional complexation was the primary source of the delayed reaction. We further compared the transient EL curves of PyPO based non-doped devices with a typical TTA device based on 2-methyl-9,10- bis(naphthalen-2-yl) anthracene (MADN) at different driving voltages. The PyPO-based devices decayed much faster than the MADN-based device after the pulse voltage was cut off. As the driving voltage ramped up from 5 V to 7 V, the ratio of the delayed fraction of the MADN-based device rapidly declined due to the enhanced triplet exciton annihilation process, which was inconsistent with PyPO-based devices. Therefore, the contribution from TTA mechanism was insignificant in the EL process. Furthermore, the determined energy gap between S_1 and T_1 was as large as 0.88 eV and an effective channel for RISC could not be established. So TADF mechanism would also be ruled out. Based on theoretical calculations, we concluded that the source of excitons should be ascribed to the high-lying triplet excitons through hRISC.

2.6. PhOLEDs using PyPO as the host

Considering the high efficient utilization of triplet excitons, PyPO was expected to be the host of phosphorescent OLEDs [55]. Two typical iridium red phosphors ($Ir(piq)_3$ and $Ir(piq)_2acac$) were chose to be the guest of PhOLEDs. The Dexter energy transfer from the T_1 of red phosphors to that of PyPO was made possible since the T_1 energy levels of two phosphors (2.0 eV) and PyPO (2.18 eV) were in good agreement. The devices were prepared with a structure of ITO/HATCN (10 nm)/TAPC (30 nm)/TCTA (10 nm)/PyPO:5 wt% emitters (20 nm)/TmPyPB (40 nm)/LiF (1 nm)/Al (120 nm), in which the emitters were $Ir(piq)_3$ for device R1 and $Ir(piq)_2acac$ for device R2, respectively. Fig. 6 and Table 3 provided illustrations and summaries of the EL performances. Low driving voltages of 3.0 V and 2.8 V allowed device R1 and R2 to be turned on, respectively. These devices exhibited ultra-vivid red emission with EL peaks at 628 nm and 632 nm, and maximum luminance of 23561 cd m^{-2} and 27344 cd m^{-2}, respectively. It was not observed any blue emission belonging to PyPO in EL spectra, which indicated that complete energy transfer at a proper doping concentration. Notably, the maximum EQEs of device R1 and device R2 were as high as 25.3% and 31.3%, respectively, representing the leading level of red phosphorescent OLEDs. Meanwhile, the unchanged EL spectra at different driving voltages implied the stable exciton recombination region in these devices (Fig. S11).

To gain an insight into the impressive EL performances of the devices R1 and R2, the absorption spectra of both phosphors was determined in comparison with the PL spectrum of PyPO (Fig. S12). Additionally, a significant overlap was observed, indicating a high possibility for effective host–guest Förster energy transfer. The long-range Förster energy transfer required a suitable distance, which the optimal doping concentration ensured. The existence of several lower-lying triplet states and the following ISC process of triplet excitons made the Dexter energy transfer between the host and phosphorescent dyes feasible as well (Fig. 6).

3. Conclusion

In conclusion, we have successfully developed an efficient deep-blue luminogen, PyPO, which contains PyI and diphenyl ether moieties, and possesses weak ICT excited state characteristic. The thin film of PyPO shows a high PLQY of 70.7% and a high horizontal dipole ratio of 84.0%.

Table 1
Summary of the photophysical, thermal, and electrochemical parameters of PyPO.

λ_{abs} (nm)	λ_{em} (nm)		Φ_F[c] (%)		τ (ns)		T_g (°C)	T_d (°C)	S_1 (eV)	T_1 (eV)	E_{LUMO}/E_{HOMO}[d] (eV)
	sol[a]	film[b]	sol[a]	film[b]	sol[a]	film[b]					
338	420	452	90.1	70.7	2.25	2.91	103	410	3.06	2.18	−2.55/−5.52

[a] Measured in tetrahydrofuran (THF) solution (1×10^{-5} M) at room temperature.
[b] Measured in a neat film.
[c] Absolute PL quantum efficiency.
[d] Determined from cyclic voltammetry measurement.

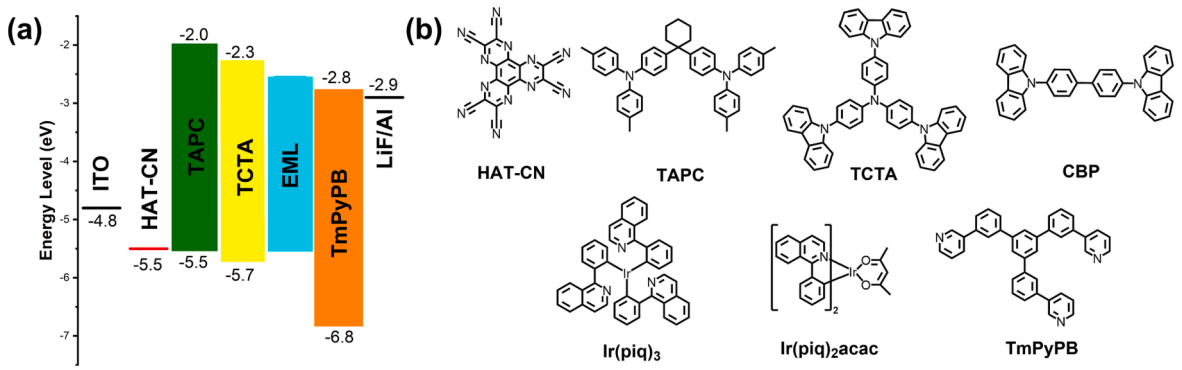

Fig. 4. (a) Energy level diagram and (b) the chemical structures of the used emitters in the devices.

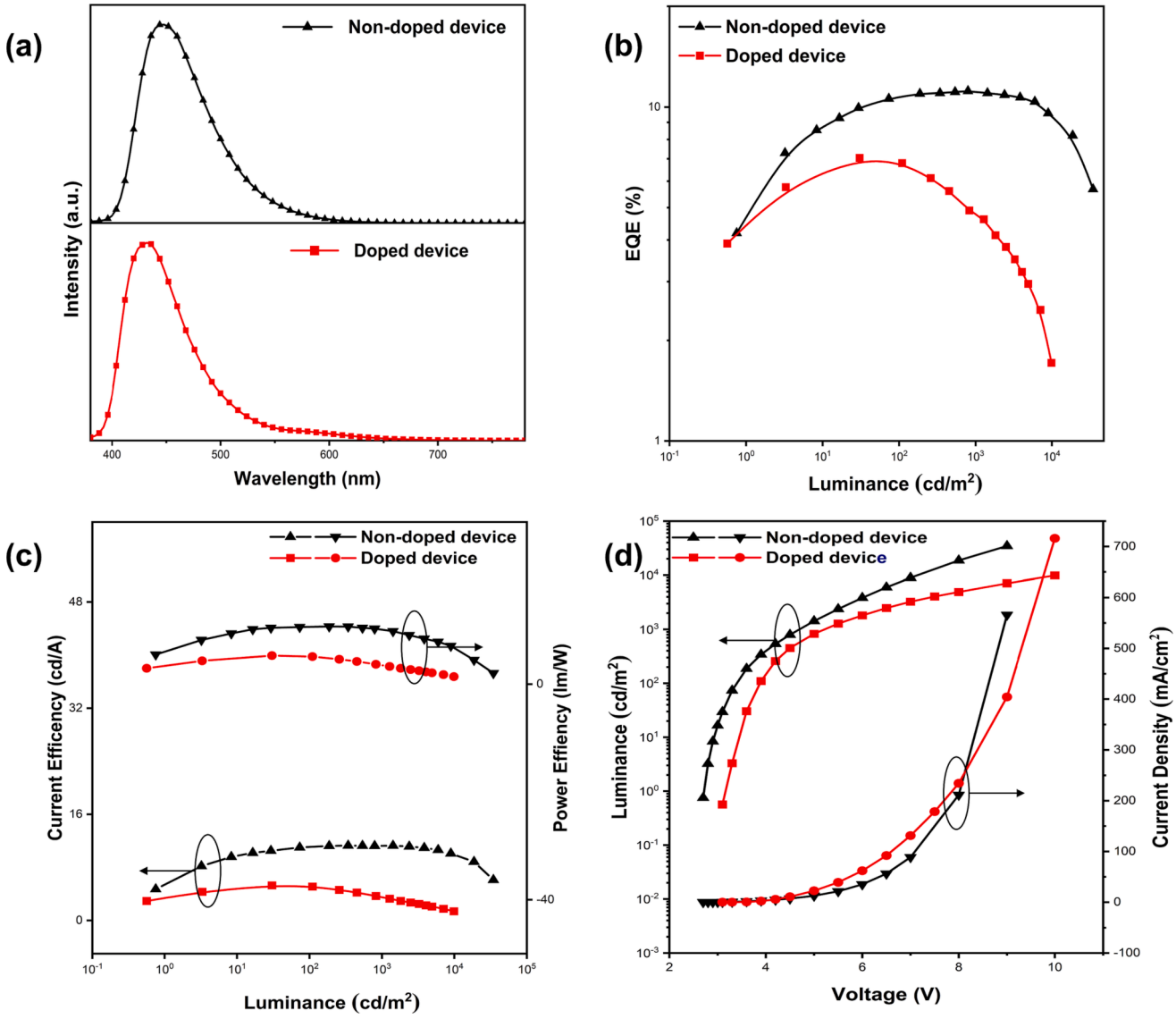

Fig. 5. Non-doped and doped devices (a) The EL spectra at 5 V. (b) The EQE-luminance curve. (c) The current density–voltage-luminance curve. (d) The current efficiency–luminance-power efficiency curve.

The non-doped device employed PyPO as emitting layer exhibits stable deep-blue emission at 448 nm with an excellent maximum EQE of 11.1% and CIE coordinates of (0.15, 0.13), which is one of the best results of non-doped devices based on PyI derivatives. The high-energy excited state investigation and transient EL decay measurement illustrate that such excellent device efficiency derives from the utilization of triplet excitons through hot exciton path. At the same time, PyPO can also be acted as the host to fabricate doped PhOLEDs. The red phosphorescent

Table 2
EL performances using PyPO as the emitter.

Device	λ_{EL}[a] (nm)	FWHM[b](nm)	V_{on}[c](V)	L_{max}[d] (cd m^{-2})	CE_{max}[e] (cd A^{-1})	PE_{max}[f] (lm W^{-1})	EQE_{max}[g](%)	Roll-off[h](%)	CIE[i] (x, y)
Non-doped	448	76	2.8	34,546	11.2	10.6	11.1	0.9/27.9	0.15, 0.13
Doped	432	66	3.2	9872	5.2	4.6	7.0	34/-	0.14, 0.07

[a] λ_{EL}: emission peak of EL spectra at 6 V.
[b] FWHM: the full width at half maxima of EL spectra.
[c] V_{on}: turn-on voltage at the luminescence of 1 cd m^{-2}.
[d] L_{max}: maximum luminance.
[e] CE_{max}: maximum current efficiency.
[f] PEmax: maximum power efficiency.
[g] EQE:maximum external quantum efficiency.
[h] Roll-off: device roll-off at 1 000 cd m^{-2}/10 000 cd m^{-2}.
[i] CIE: Commission International de l'Eclairage (CIE) coordinates at 6 V.

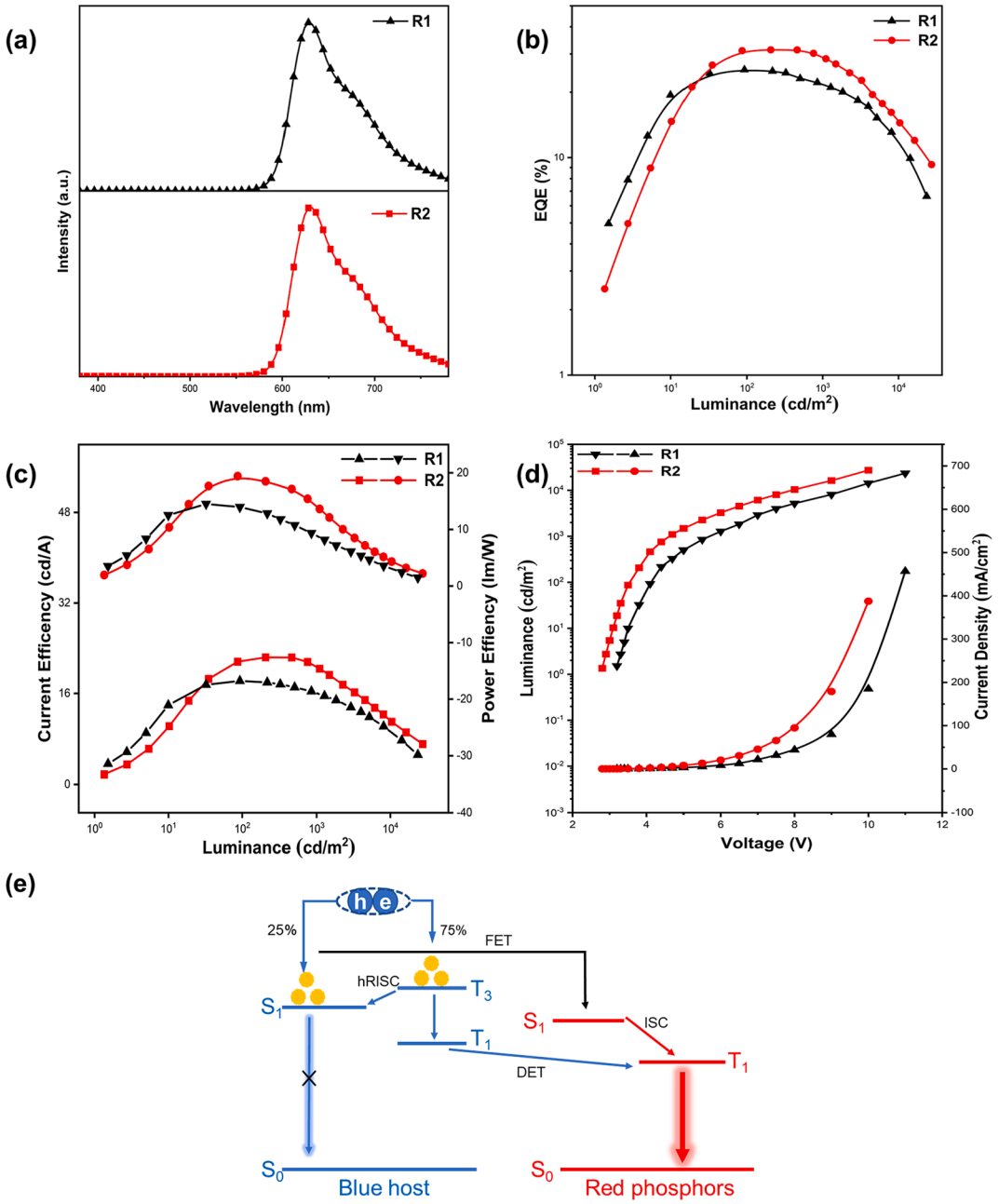

Fig. 6. Device R1 and R2 (a) The EL spectra at 6 V. (b) The EQE-luminance curve. (c) The current density–voltage-luminance curve. (d) The current efficiency-luminance-power efficiency curve of R1 and R2. (e) Proposed mechanism of the PhOLEDs utilizing PyPO as the host. Abbreviations: FET = Förster energy transfer; DET = Dexter energy transfer; ISC = Intersystem crossing.

Table 3
EL performances of PhOLEDs using PyPO as the host.

Device	λ_{EL}[a] (nm)	FWHM[b](nm)	V_{on}[c] (V)	L_{max}[d] (cd m^{-2})	CE_{max}[e] (cd A^{-1})	PE_{max}[f] (lm W^{-1})	EQE[g] (%)	Roll-off[h] (%)	CIE[i] (x, y)
R1	628	84	3.0	23,561	18.2	14.5	25.3	16.9/43.4	0.67, 0.32
R2	632	78	2.8	27,344	22.3	19.4	31.3	8.9/53.9	0.67, 0.31

[a] λ_{EL}: emission peak of EL spectra at 6 V.
[b] FWHM: the full width at half maxima of EL spectra.
[c] V_{on}: turn-on voltage at the luminescence of 1 cd m^{-2}.
[d] L_{max}: maximum luminance.
[e] CE_{max}: maximum current efficiency.
[f] PE_{max}: maximum power efficiency.
[g] EQE:maximum external quantum efficiency.
[h] Roll-off: device roll-off at 1 000 cd m^{-2}/10 000 cd m^{-2}.
[i] CIE: Commission International de l'Eclairage (CIE) coordinates at 6 V.

device using $Ir(piq)_3$ as dopant achieves the maximum EQE of 31.3%. These results provide an inspiring way for the preparation of high-efficiency deep-blue materials applicable in non-doped OLEDs.

Declaration of Competing Interest

The authors declare that they have no known competing financial interests or personal relationships that could have appeared to influence the work reported in this paper.

Data availability

No data was used for the research described in the article.

Acknowledgements

This research is supported by the National Natural Science Foundation of China (22075100), Jilin Provincial Science and Technology Department (20220201082GX) and State Key Laboratory of Luminescence and Applications (SKLA-2020-01).

Appendix A. Supplementary data

Supplementary data to this article can be found online at https://doi.org/10.1016/j.cej.2023.145867.

References

[1] C.W. Tang, S.A. VanSlyke, Organic electroluminescent diodes, Appl. Phys. Lett. 51 (12) (1987) 913–915.
[2] M.A. Baldo, D.F. O'Brien, Y. You, A. Shoustikov, S. Sibley, M.E. Thompson, S. R. Forrest, Highly efficient phosphorescent emission from organic electroluminescent devices, Nature 395 (6698) (1998) 151–154.
[3] M. Zhu, C. Yang, Blue fluorescent emitters: design tactics and applications in organic light-emitting diodes, Chem. Soc. Rev. 42 (12) (2013) 4963–4976, https://doi.org/10.1039/c3cs35440g.
[4] H.W. Chen, J.H. Lee, B.Y. Lin, S. Chen, S.T. Wu, Liquid crystal display and organic light-emitting diode display: present status and future perspectives, Light Sci. Appl. 7 (2018) 17168, https://doi.org/10.1038/lsa.2017.168.
[5] T. Liu, L. Zhu, C. Zhong, G. Xie, S. Gong, J. Fang, D. Ma, C. Yang, Naphthothiadiazole-Based Near-Infrared Emitter with a Photoluminescence Quantum Yield of 60% in Neat Film and External Quantum Efficiencies of up to 3.9% in Nondoped OLEDs, Adv. Funct. Mater. 27 (12) (2017) 1606384.
[6] W. Song, L. Shi, L. Gao, P. Hu, H. Mu, Z. Xia, J. Huang, J. Su, [1,2,4]Triazolo[1,5-a] pyridine as Building Blocks for Universal Host Materials for High-Performance Red Green, Blue and White Phosphorescent Organic Light-Emitting Devices, ACS Appl. Mater. Interfaces 10 (6) (2018) 5714–5722, https://doi.org/10.1021/acsami.7b18202.
[7] Z. Xu, J. Gu, X. Qiao, A. Qin, B.Z. Tang, D. Ma, Highly Efficient Deep Blue Aggregation-Induced Emission Organic Molecule: A Promising Multifunctional Electroluminescence Material for Blue/Green/Orange/Red/White OLEDs with Superior Efficiency and Low Roll-Off, ACS Photonics 6 (3) (2019) 767–778, https://doi.org/10.1021/acsphotonics.8b01724.
[8] A. Abdurahman, T.J.H. Hele, Q. Gu, J. Zhang, Q. Peng, M. Zhang, R.H. Friend, F. Li, E.W. Evans, Understanding the luminescent nature of organic radicals for efficient doublet emitters and pure-red light-emitting diodes, Nat. Mater. 19 (11) (2020) 1224–1229, https://doi.org/10.1038/s41563-020-0705-9.
[9] F. Liu, Z. Cheng, L. Wan, L. Gao, Z. Yan, D. Hu, L. Ying, P. Lu, Y. Ma, Anthracene-based emitters for highly efficient deep blue organic light-emitting diodes with narrow emission spectrum, Chem. Eng. J. 426 (2021) 131351.
[10] S.O. Jeon, K.H. Lee, J.S. Kim, S.G. Ihn, Y.S. Chung, J.W. Kim, H. Lee, S. Kim, H. Choi, J.Y. Lee, High-efficiency, long-lifetime deep-blue organic light-emitting diodes, Nat. Photon. 15 (3) (2021) 208–215, https://doi.org/10.1038/s41566-021-00763-5.
[11] C.J. Zheng, J. Wang, J. Ye, M.F. Lo, X.K. Liu, M.K. Fung, X.H. Zhang, C.S. Lee, Novel efficient blue fluorophors with small singlet-triplet splitting: hosts for highly efficient fluorescence and phosphorescence hybrid WOLEDs with simplified structure, Adv. Mater. 25 (15) (2013) 2205–2211, https://doi.org/10.1002/adma.201204724.
[12] D. Volyniuk, V. Cherpak, P. Stakhira, B. Minaev, G. Baryshnikov, M. Chapran, A. Tomkeviciene, J. Keruckas, J.V. Grazulevicius, Highly Efficient Blue Organic Light-Emitting Diodes Based on Intermolecular Triplet-Singlet Energy Transfer, J. Phys. Chem. C 117 (44) (2013) 22538–22544, https://doi.org/10.1021/jp407397y.
[13] S. Zhang, L. Yao, Q. Peng, W. Li, Y. Pan, R. Xiao, Y. Gao, C. Gu, Z. Wang, P. Lu, F. Li, S. Su, B. Yang, Y. Ma, Achieving a Significantly Increased Efficiency in Nondoped Pure Blue Fluorescent OLED: A Quasi-Equivalent Hybridized Excited State, Adv. Funct. Mater. 25 (11) (2015) 1755–1762, https://doi.org/10.1002/adfm.201404260.
[14] H. Liu, Q. Bai, L. Yao, H. Zhang, H. Xu, S. Zhang, W. Li, Y. Gao, J. Li, P. Lu, H. Wang, B. Yang, Y. Ma, Highly efficient near ultraviolet organic light-emitting diode based on a meta-linked donor-acceptor molecule, Chem. Sci. 6 (7) (2015) 3797–3804, https://doi.org/10.1039/c5sc01131k.
[15] Y. Chen, J. Zhu, Y. Wu, J. Yao, D. Yang, X. Qiao, Y. Dai, Q. Tong, D. Ma, Highly efficient fluorescence/phosphorescence hybrid white organic light-emitting devices based on a bipolar blue emitter to precisely control charges and excitons, J. Mater. Chem. C 8 (22) (2020) 7543–7551, https://doi.org/10.1039/d0tc01549k.
[16] R.R. Søndergaard, M. Hösel, F.C. Krebs, Roll-to-Roll fabrication of large area functional organic materials, J Polym Sci B 51 (1) (2013) 16–34, https://doi.org/10.1002/polb.23192.
[17] H. Liu, L. Kang, J. Li, F. Liu, X. He, S. Ren, X. Tang, C. Lv, P. Lu, Highly efficient deep-blue organic light-emitting diodes based on pyreno[4,5-d]imidazole-anthracene structural isomers, J. Mater. Chem. C 7 (33) (2019) 10273–10280, https://doi.org/10.1039/c9tc02990g.
[18] X.Y. Wang, J. Gong, H. Zou, S.H. Liu, J. Zhang, Aggregation-induced conversion from TADF to phosphorescence of gold(I) complexes with millisecond lifetimes, Aggregate 4 (2) (2022), https://doi.org/10.1002/agt2.252.
[19] Y. Sun, D. Zhong, S. Liu, L. Yue, Z. Feng, X. Deng, X. Chen, X. Yang, G. Zhou, Achieving highly efficient bipolar near-ultraviolet emitters via regulating the energy levels of the excited states by a co-acceptor system, J. Mater. Chem. C 11 (14) (2023) 4694–4702, https://doi.org/10.1039/d3tc00147d.
[20] Y. Ma, H. Zhang, J. Shen, C. Che, Electroluminescence from Triplet Metal-Ligand Charge-Transfer Excited State of Transition Metal Complexes, Synth. Met. 94 (3) (1998) 245–248.
[21] Y. Ma, X. Zhou, J. Shen, H.-Y. Chao, Triplet luminescent dinuclear-gold(I) complex-based light-emitting diodes with low turn-on voltage, Appl. Phys. Lett. 74 (10) (1999) 1361–1363.
[22] C. Ulbricht, B. Beyer, C. Friebe, A. Winter, U.S. Schubert, Recent Developments in the Application of Phosphorescent Iridium(III) Complex Systems, Adv. Mater. 21 (44) (2009) 4418–4441, https://doi.org/10.1002/adma.200803537.
[23] N.C.G. Y. R. Sun, H. Kanno, B.W. Ma, M. E. Thompson, a.S.R. Forrest, Management of singlet and triplet excitons for efficient white organic light-emitting devices, Nature 440 (2006) 908–912. https://doi.org/https://doi.org/10.1038/nature04645.
[24] G. Mehes, H. Nomura, Q. Zhang, T. Nakagawa, C. Adachi, Enhanced electroluminescence efficiency in a spiro-acridine derivative through thermally activated delayed fluorescence, Angew. Chem. Int. Ed. Engl. 51 (45) (2012) 11311–11315, https://doi.org/10.1002/anie.201206289.
[25] P. Han, C. Lin, D. Ma, A. Qin, B.Z. Tang, Violet-Blue Emitters Featuring Aggregation-Enhanced Emission Characteristics for Nondoped OLEDs with CIEy Smaller than 0.046, ACS Appl. Mater. Interfaces 12 (41) (2020) 46366–46372, https://doi.org/10.1021/acsami.0c12722.

[26] X. Tang, Q. Bai, T. Shan, J. Li, Y.u. Gao, F. Liu, H. Liu, Q. Peng, B. Yang, F. Li, P. Lu, Efficient Nondoped Blue Fluorescent Organic Light-Emitting Diodes (OLEDs) with a High External Quantum Efficiency of 9.4% @ 1000 cd/m^{-2}(−|) Based on Phenanthroimidazole−Anthracene Derivative, Adv. Funct. Mater. 28 (11) (2018) 1705813.
[27] Y. Liu, F. Liang, L.-S. Cui, X.-B. Shi, Z.-K. Wang, L.-S. Liao, Simplified Hybrid White Organic Light-Emitting Diodes with a Mixed Fluorescent Blue Emitting Layer for Exciton Managing and Lifetime Improving, Adv. Opt. Mater. 4 (12) (2016) 2051–2056, https://doi.org/10.1002/adom.201600410.
[28] S. Chen, J. Lian, W. Wang, Y. Jiang, X. Wang, S. Chen, P. Zeng, Z. Peng, Efficient deep blue electroluminescence with CIEy ∈ (0.05–0.07) from phenanthroimidazole–acridine derivative hybrid fluorophores, J. Mater. Chem. C 6 (35) (2018) 9363–9373, https://doi.org/10.1039/c8tc02954g.
[29] D. Zhong, X. Yang, X. Deng, X.i. Chen, Y. Sun, P. Tao, Z. Li, J. Zhang, G. Zhou, W.-Y. Wong, Achieving highly efficient near-ultraviolet emitters via optimizing molecular configuration by the intramolecular-locked donor and acceptor, Chem. Eng. J. 452 (2023) 139480.
[30] X. Qiu, Y. Xu, C. Wang, M. Hanif, J. Zhou, C. Zeng, Y. Li, Q. Jiang, R. Zhao, D. Hu, Y. Ma, Synergistic effects of hydrogen bonds and the hybridized excited state observed for high-efficiency, deep-blue fluorescent emitters with narrow emission in OLED applications, J. Mater. Chem. C 7 (18) (2019) 5461–5467, https://doi.org/10.1039/c9tc00357f.
[31] R. Kim, S. Lee, K.H. Kim, Y.J. Lee, S.K. Kwon, J.J. Kim, Y.H. Kim, Extremely deep blue and highly efficient non-doped organic light emitting diodes using an asymmetric anthracene derivative with a xylene unit, Chem. Commun. (Camb) 49 (41) (2013) 4664–4666, https://doi.org/10.1039/c3cc41441h.
[32] X. Chen, S. Liu, Y. Sun, D. Zhong, Z. Feng, X. Yang, B. Su, Y. Sun, G. Zhou, B. Jiao, Z. Wu, Blue emitters with various electron-donors attached to the 9-phenyl-9-phosphafluorene oxide (PhFIOP) moiety and their thermally activated delayed fluorescence (TADF) behavior, Mater. Chem. Front. 7 (9) (2023) 1841–1854, https://doi.org/10.1039/d2qm01339h.
[33] K.H. Kim, J.Y. Baek, C.W. Cheon, C.K. Moon, B. Sim, M.Y. Choi, J.J. Kim, Y.H. Kim, Highly efficient non-doped deep blue fluorescent emitters with horizontal emitting dipoles using interconnecting units between chromophores, Chem. Commun. (Camb) 52 (73) (2016) 10956–10959, https://doi.org/10.1039/c6cc05076j.
[34] W. Li, L. Yao, H. Liu, Z. Wang, S. Zhang, R. Xiao, H. Zhang, P. Lu, B. Yang, Y. Ma, Highly efficient deep-blue OLED with an extraordinarily narrow FHWM of 35 nm and a y coordinate <0.05 based on a fully twisting donor–acceptor molecule, J. Mater. Chem. C 2(24) (2014) 4733-4736. https://doi.org/10.1039/c4tc00487f.
[35] R.K. Konidena, J. Lim, J.Y. Lee, A novel molecular design featuring the conversion of inefficient TADF emitters into efficient TADF emitters for deep-blue organic light emitting diodes, Chem. Eng. J. 416 (2021) 129097.
[36] H. Uoyama, K. Goushi, K. Shizu, H. Nomura, C. Adachi, Highly efficient organic light-emitting diodes from delayed fluorescence, Nature 492 (7428) (2012) 234–238, https://doi.org/10.1038/nature11687.
[37] C. Yin, D. Zhang, Y. Zhang, Y. Lu, R. Wang, G. Li, L. Duan, High-Efficiency Narrow-Band Electro-Fluorescent Devices with Thermally Activated Delayed Fluorescence Sensitizers Combined Through-Bond and Through-Space Charge Transfers CCS, Chem. 2 (4) (2020) 1268–1277. https://doi.org/10.31635/ccschem.020.202000243.
[38] Q. Zhang, J. Li, K. Shizu, S. Huang, S. Hirata, H. Miyazaki, C. Adachi, Design of efficient thermally activated delayed fluorescence materials for pure blue organic light emitting diodes, J. Am. Chem. Soc. 134 (36) (2012) 14706–14709, https://doi.org/10.1021/ja306538w.
[39] D.H. Ahn, S.W. Kim, H. Lee, I.J. Ko, D. Karthik, J.Y. Lee, J.H. Kwon, Highly efficient blue thermally activated delayed fluorescence emitters based on symmetrical and rigid oxygen-bridged boron acceptors, Nat. Photon. 13 (8) (2019) 540–546, https://doi.org/10.1038/s41566-019-0415-5.
[40] M. Godumala, S. Choi, M.J. Cho, D.H. Choi, Recent breakthroughs in thermally activated delayed fluorescence organic light emitting diodes containing non-doped emitting layers, J. Mater. Chem. C 7 (8) (2019) 2172–2198, https://doi.org/10.1039/c8tc06293e.
[41] Z. Huang, B. Lei, D. Yang, D. Ma, Z. Bin, J. You, Modified Intramolecular-Lock Strategy Enables Efficient Thermally Activated Delayed Fluorescence Emitters for Non-Doped OLEDs, Angew. Chem. Int. Ed. Engl. 61 (50) (2022) e202213157.
[42] W. Li, Y. Pan, L. Yao, H. Liu, S. Zhang, C. Wang, F. Shen, P. Lu, B. Yang, Y. Ma, A Hybridized Local and Charge-Transfer Excited State for Highly Efficient Fluorescent OLEDs: Molecular Design, Spectral Character, and Full Exciton Utilization, Adv. Opt. Mater. 2 (9) (2014) 892–901, https://doi.org/10.1002/adom.201400154.
[43] S. Xiao, Y. Gao, R. Wang, H. Liu, W. Li, C. Zhou, S. Xue, S.-T. Zhang, B. Yang, Y. Ma, Highly efficient hybridized local and Charge-transfer (HLCT) Deep-blue electroluminescence with excellent molecular horizontal orientation, Chem. Eng. J. 440 (2022) 135911.
[44] H. Zhang, G. Li, X. Guo, K. Zhang, B. Zhang, X. Guo, Y. Li, J. Fan, Z. Wang, D. Ma, B.Z. Tang, High-Performance Ultraviolet Organic Light-Emitting Diode Enabled by High-Lying Reverse Intersystem Crossing, Angew. Chem. Int. Ed. Engl. 60 (41) (2021) 22241–22247, https://doi.org/10.1002/anie.202108540.
[45] W. Cui, C. Liu, X. Chao, M. Xie, Q. Sun, D. Liu, Y. Pan, S.T. Zhang, S. Xue, W. Yang, Highly Efficient Blue Electro-Fluorescence and Hybrid White Electroluminescence Basing on a Novel Hybrid Local and Charge-Transfer (HLCT) Material with Weak Donor-Acceptor Structure and High Carrier Mobilities, Advanced, Opt. Mater. 11 (8) (2023), https://doi.org/10.1002/adom.202202947.
[46] T. Liu, X. Chen, J. Zhao, W. Wei, Z. Mao, W. Wu, S. Jiao, Y. Liu, Z. Yang, Z. Chi, Hybridized local and charge-transfer excited state fluorophores enabling organic light-emitting diodes with record high efficiencies close to 20, Chem. Sci. 12 (14) (2021) 5171–5176, https://doi.org/10.1039/d1sc00272d.
[47] X. Lv, M. Sun, L. Xu, R. Wang, H. Zhou, Y. Pan, S. Zhang, Q. Sun, S. Xue, W. Yang, Highly efficient non-doped blue fluorescent OLEDs with low efficiency roll-off based on hybridized local and charge transfer excited state emitters, Chem. Sci. 11 (19) (2020) 5058–5065, https://doi.org/10.1039/d0sc01341b.
[48] H. Hwang, Y.S. Shim, J. Choi, D.J. Lee, J.G. Kim, J.S. Lee, Y.W. Park, B.K. Ju, Nano-arrayed OLEDs: enhanced outcoupling efficiency and suppressed efficiency roll-off, Nanoscale 10 (41) (2018) 19330–19337, https://doi.org/10.1039/c8nr03198c.
[49] X. Tang, L.S. Cui, H.C. Li, A.J. Gillett, F. Auras, Y.K. Qu, C. Zhong, S.T.E. Jones, Z. Q. Jiang, R.H. Friend, L.S. Liao, Highly efficient luminescence from space-confined charge-transfer emitters, Nat. Mater. 19 (12) (2020) 1332–1338, https://doi.org/10.1038/s41563-020-0710-z.
[50] X. Lv, L. Xu, M. Cang, R. Wang, M. Sun, H. Zhou, Y. Yu, Q. Sun, Y. Pan, Y. Xu, D. Hu, S. Xue, W. Yang, Pure-Blue Fluorescence Molecule for Nondoped Electroluminescence with External Quantum Efficiency Approaching 13%, CCS. Chem. 3 (9) (2021) 2557–2568. https://doi.org/10.31635/ccschem.020.202000392.
[51] F. Liu, H. Liu, X. Tang, S. Ren, X. He, J. Li, C. Du, Z. Feng, P. Lu, Novel blue fluorescent materials for high-performance nondoped blue OLEDs and hybrid pure white OLEDs with ultrahigh color rendering index, Nano Energy 68 (2020) 104325.
[52] G. Yang, Y. Ran, Y. Wu, M. Chen, Z. Bin, J. You, Endowing imidazole derivatives with thermally activated delayed fluorescence and aggregation-induced emission properties for highly efficient non-doped organic light-emitting diodes, Aggregate 3 (2) (2021), https://doi.org/10.1002/agt2.127.
[53] Q. Zhang, H. Kuwabara, W.J. Potscavage, S. Huang, Y. Hatae, T. Shibata, C. Adachi, Anthraquinone-based intramolecular charge-transfer compounds: Computational molecular design, thermally activated delayed fluorescence, and highly efficient red electroluminescence, J. Am. Chem. Soc. 136 (52) (2014) 18070–18081, https://doi.org/10.1021/ja510144h.
[54] Q.S. Zhang, B. Li, S.P. Huang, H. Nomura, H. Tanaka, C. Adachi, Efficient blue organic light-emitting diodes employing thermally activated delayed fluorescence, Nat. Photon. 8 (4) (2014) 326–332, https://doi.org/10.1038/Nphoton.2014.12.
[55] Y. Tao, C. Yang, J. Qin, Organic host materials for phosphorescent organic light-emitting diodes, Chem. Soc. Rev. 40 (5) (2011) 2943–2970, https://doi.org/10.1039/c0cs00160k.